Supplement of Geosci. Model Dev., 17, 4311–4330, 2024
https://doi.org/10.5194/gmd-17-4311-2024-supplement

Geoscientific Model Development
Open Access
EGU

Supplement of

Development of a multiphase chemical mechanism to improve secondary organic aerosol formation in CAABA/MECCA (version 4.7.0)

Felix Wieser et al.

Correspondence to: Felix Wieser (f.wieser@fz-juelich.de) and Domenico Taraborrelli (d.taraborrelli@fz-juelich.de)

Supplement "Development of a chemical mechanism to improve secondary organic aerosol formation in the box model CAABA/MECCA (version 4.7.0)"

Contents

S1. Reaction rate constants

Table S1. Summary of rate constants and substituent factors used in the new mechanism. (adapted from Sander et al. (2019))

Variable	Rate constant / substituent factor	Description / substituent
H-abstraction by OH		
k_p	$4.49 \times 10^{-18} \times T^2 \times \exp(-320/T)$	Primary H-abstraction
k_s	$4.50 \times 10^{-18} \times T^2 \times \exp(253/T)$	Secondary H-abstraction
k_t	$2.12 \times 10^{-18} \times T^2 \times \exp(696/T)$	Tertiary H-abstraction
Substituent factor f		
f_{sOH}	3.44	OH at sec. carbon
f_{tOH}	2.68	OH at tert. carbon
f_{sOOH}	8.00	OOH at tert. carbon
f_{tOOH}	8.00	OOH at sec. carbon
f_{CHO}	0.55	aldehyde
f_{CO2H}	1.67	carbonic acid
f_O	8.15	double bond to O
OH-addition to double bonds		
k_{adp}	$4.5 \times 10^{-12} \times (T/300)^{-0.85}$	primary carbon of double bond
k_{ads}	$0.25 \times (1.1 \times 10^{-11} \times \exp(485/T)$ $+1.0 \times 10^{-11} \times \exp(553/T))$	secondary carbon of double bond
k_{adt}	$1.92 \times 10^{-11} \times \exp(450/T) - k_{ads}$	tertiary carbon of double bond
Substituent factor a		
a_{CHO}	0.31	aldehyde
a_{COCH3}	0.76	ketone
a_{CH2OH}	1.7	alcohol
a_{CH2OOH}	1.7	hydroperoxide
NO reaction with peroxy radicals		
k_{RO2NO}	$2.54 \times 10^{-12} \times \exp(360/T)$	all branches (NO-add. & O-abst.)
HO_2 reaction with peroxy radicals		
k_{RO2HO2}	$2.91 \times 10^{-13} \times \exp(1300/T) \times$ $(1 - \exp(-0.245 \times n_C))$	all branches (H-add. & O-abst.) n_C = number of carbon
HO_2 reaction with peroxy radicals		
k_{RO2NO3}	2.30×10^{-12}	O-abstraction
H abstraction to OOH by OH		
k_{ROOHRO}	$0.6 \times (5.3 \times 10^{-12} \times \exp(190/T))$	H-abstraction only OOH

S2. Reaction mechanism

S2.1. Isoprene

S2.1.1. OH-pathway

Main developments of the OH-pathway concern the formation and degradation of epoxides. IEPOX formation based on Paulot et al. (2009) was previously introduced to the model, together with the generation of the precursor isoprene hydroxy hydroperoxide (ISOPBOOH) (Taraborrelli et al., 2012; Sander et al., 2019). New to the mechanism is the division of the lumped IEPOX into the three main isomers (implemented with 85% branching ratio of the ISOPBOOH OH-oxidation). The mechanism considers cis-IEPOX, trans-IEPOX, and δ-IEPOX. cis-IEPOX and trans-IEPOX exhibit the same reaction scheme with adapted reaction rates. The delta-IEPOX scheme is simplified due to its low yield. Products of δ-IEPOX are methylglyoxal and acetol (Not shown).

The formation of a dihydroxy hydroperoxy peroxide (15% branching ratio of the ISOPBOOH OH-oxidation) is competing with the IEPOX formation, resulting in an epoxide (ISOPBEPX) after ring closure (see Fig. S2, step 1-4) (D'Ambro et al., 2017). Similar to IEPOX, the H-shift is treated explicitly (rate-determining), and the ring closure is considered instantaneous ($\sim 1\times10^{-2}$ vs 9×10^{9} s^{-1}). LISOPBEPX is low-volatile and partitions to available aqueous-phase (H_s = $1.3\times10^{10}\mathrm{M/atm}$). The subsequent degradation is developed from Cope et al. (2021). In the mechanism, the H-abstraction is explicitly modeled, while the ring-opening is not independently considered. The rate constant is calculated by the estimation scheme of Monod and Doussin (2008). The scheme does not cover epoxides, thus the activity coefficient is assumed to be similar to an alcohol group. Following the CLEPS scheme (Mouchel-Vallon et al., 2017), peroxy radicals in the aqueous phase react by RO_2 self-reaction and resulting alkoxy radicals perform a β-scission.

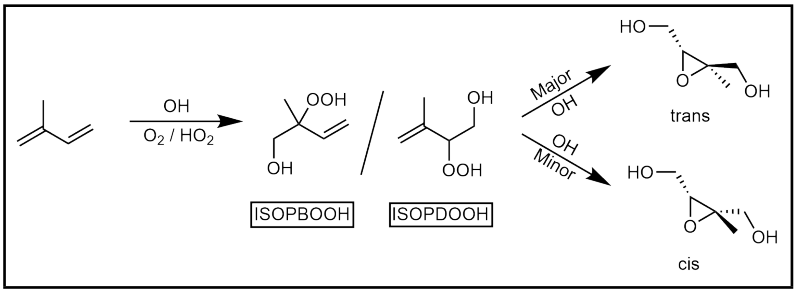

Figure S1. Isoprene oxidation pathway resulting in the formation of trans- and cis-IEPOX. Only the major Isomers of ISOPOOH (center) are shown, but all isomers as well as the corresponding products are implemented into MECCA. In chamber experiments 33% trans- and 67% cis-IEPOX (1,2-ISOPOOH) is produced, while the formation ratio is depending on the observed ISOPOOH isomere (St. Clair et al., 2016; Bates et al., 2014).

Fig. S1 mechanism in kpp format: (LISOPACOOH and ISOPDOOH already formed in old mechanism)

```
#REPLACE <G45026a>
<G45026a> ISOPBOOH + OH   = .85 TBIEPOX + .85 OH + .15 LISOPBOOHO2 : {%TrG} 0.67*(k_ads)*a_CH2OOH*a_CH2OH;
#ENDREPLACE
#REPLACE <>
<G45026d> ISOPBOOH + OH   = .85 CBIEPOX + .85 OH + .15 LISOPBOOHO2 : {%TrG} 0.33*(k_ads)*a_CH2OOH*a_CH2OH;
#ENDREPLACE
#REPLACE <G45034a>
<G45034a> ISOPDOOH + OH   = .85 TBIEPOX + .85 OH + .15 LISOPBOOHO2 : {%TrG} 0.68*(k_adt)*a_CH2OOH*a_CH2OH;
#ENDREPLACE
#REPLACE <>
<G45034e> ISOPDOOH + OH   = .85 CBIEPOX + .85 OH + .15 LISOPBOOHO2 : {%TrG} 0.32*(k_adt)*a_CH2OOH*a_CH2OH;
#ENDREPLACE
```

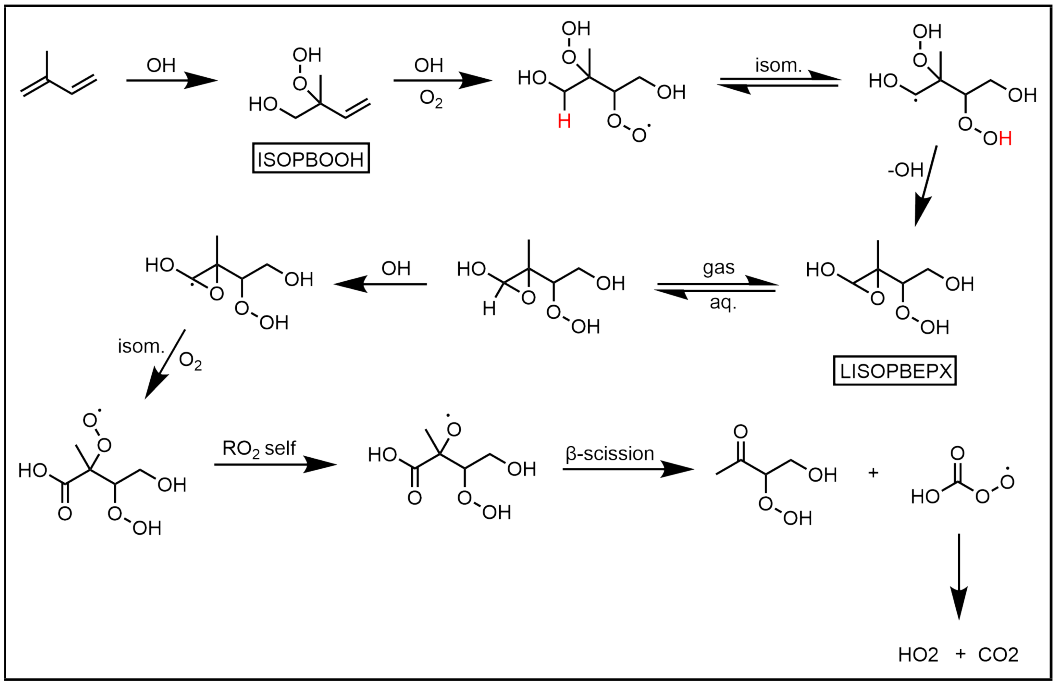

Figure S2. Isoprene OH oxidation referring to results by D'Ambro et al. (2017) and further aqueous degradation adapted from Cope et al. (2021). Not all implemented reactions are shown in the scheme.

Fig. S2 mechanism in kpp format: (ISOPBOOH already formed in old mechanism; LISOPBOOHO2 from above)

```
#REPLACE <>
<G45985> LISOPBOOHO2     = LISOPBEPX + OH                                  : {%TrG} 8.05E-2*temp**(3.81)*EXP(-7026/temp);
#ENDREPLACE
#REPLACE <>
<A45014_a##> LISOPBEPX_a## + OH_a## = COCOOCO2CCOOH_a## + H2O_a##            : {%TrAa##} xaer(##){§}* 2.76E9 *cvfac(##);
<A45015_a##> 2 COCOOCO2CCOOH_a##    = 2 CCOCOOCO_a## + 2 HO2_a## + 2 CO2_a## : {%TrAa##} xaer(##){§}* 1.6E8 *cvfac(##);
#ENDREPLACE
```

S2.1.2. IEPOX gas-phase

Bates et al. (2014) described the gas phase degradation of IEPOX. We adapted branching ratios and total reaction rates of cis- and trans-IEPOX. The remaining reaction rates were applied from Tab. S1 or calculated by SAR (Vereecken and Nozière, 2020). In addition to the scheme by Bates et al., we developed degradation mechanisms for chemically stable products. The main products of the mechanism are acetol, glyoxal, methylglyoxal, and various nitrates and hydroperoxides. Most products are similarly formed by the isoprene + OH scheme in the mechanisms. Therefore, the main impact on gas phase oxidation mixing ratios of isoprene is the loss of products to the aqueous-phase partitioning of IEPOX.

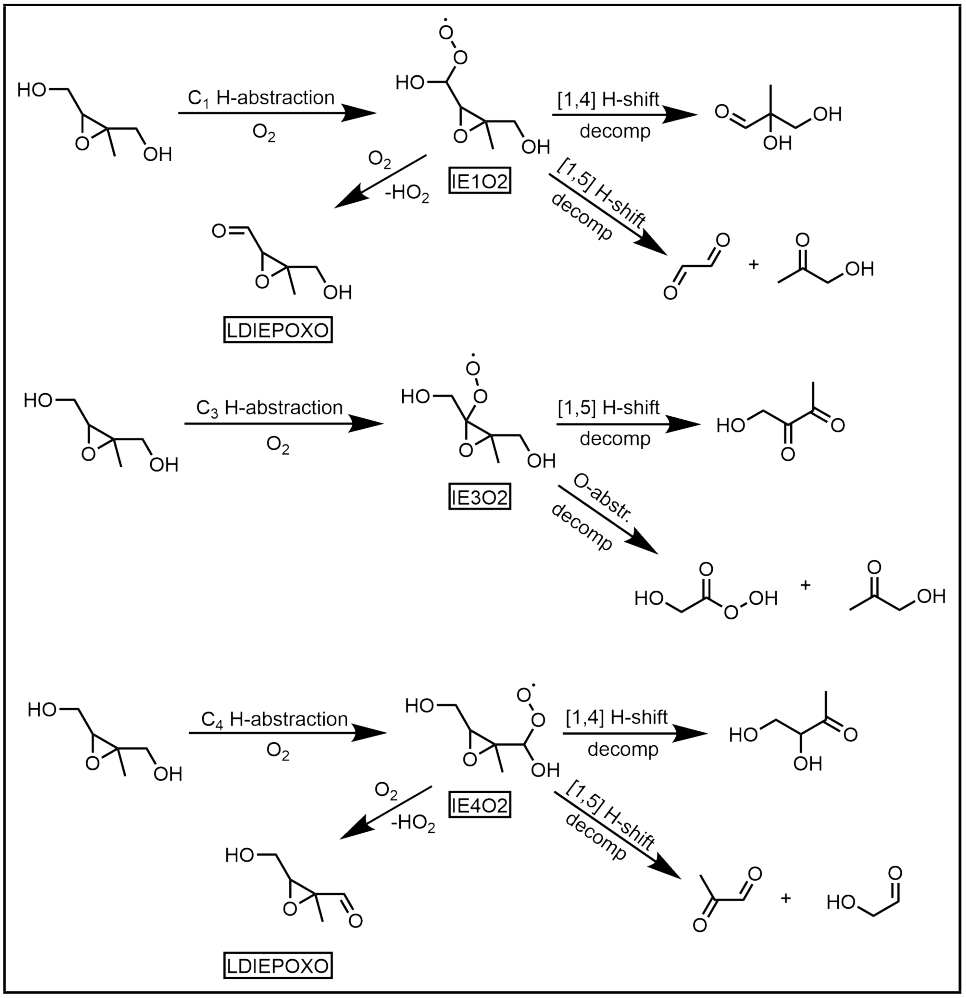

Figure S3. Simplified mechanism of the IEPOX gas-phase oxidation. H-abstraction is shown for the three main abstraction sites at C1, C3 and C4. Formed alkyl nitrates and hydroperoxides are not displayed. The aldehyde directly formed from IEPOX (IEPOXO) is lumped into one species. The degradation of the lumped IEPOXO is considered. A similar mechanism is implemented for delta-IEPOX. Not all implemented reactions are shown in the scheme.

Fig. S3 mechanism in kpp format:

```
#REPLACE <>
<G45154> CBIEPOX + OH {+O2} = .894 IE1O2 + .106 LIEPOXO +  H2O + .106 HO2 : {%TrG} k_s * f_sOH;
<G45155> CBIEPOX + OH {+O2} = .894 IE4O2 + .106 LIEPOXO +  H2O + .106 HO2 : {%TrG} k_s * f_sOH;
<G45156> CBIEPOX + OH {+O2} = IE3O2 + H2O                                 : {%TrG} (1.52E-11 - (2*k_s*f_sOH));
<G45157> TBIEPOX + OH {+O2} = .894 IE1O2 + .106 LIEPOXO +  H2O + .106 HO2 : {%TrG} k_s * f_sOH;
<G45158> TBIEPOX + OH {+O2} = .894 IE4O2 + .106 LIEPOXO +  H2O + .106 HO2 : {%TrG} k_s * f_sOH;
<G45159> TBIEPOX + OH {+O2} = IE3O2 + H2O                                 : {%TrG} (0.98E-11 - (2*k_s*f_sOH));
#ENDREPLACE
// DEGREDATION OF IE4O2
#REPLACE <>
<G45160a> IE4O2             = GLYOX + ACETOL + OH              : {%TrG} 8.05E-2 * (temp)**3.81 * EXP(-7026/temp);
<G45160b> IE4O2             = OH + CO + MACROH                 : {%TrG} 1.08E-33 * 1E-33 * (temp)**25.23 * EXP(1616/temp);
<G45160c> IE4O2 + NO        = NO2 + GLYOX + ACETOL + HO2       : {%TrG} KRO2NO * (1.-alpha_AN(9,2,1,0,0,temp,cair));
<G45160d> IE4O2 + NO        = IE4ONO2                          : {%TrG} KRO2NO * (alpha_AN(9,2,1,0,0,temp,cair));
<G45160e> IE4O2 + HO2       = IE4OOH {+O2}                     : {%TrG} 0.5*k_RO2_HO2(temp,5);
<G45160f> IE4O2 + HO2       = OH + GLYOX + ACETOL {+O2} + HO2  : {%TrG} 0.5*k_RO2_HO2(temp,5);
<G45160g> IE4O2 {+RO2}      = GLYOX + ACETOL + H2O             : {%TrG} k1_RO2sRO2;
#ENDREPLACE
// DEGREDATION OF IE3O2
#REPLACE <>
<G45161a> IE3O2             = OH + HCHO + BIACETOH             : {%TrG} 8.05E-2 * (temp)**3.81 * EXP(-7326/temp);
<G45161b> IE3O2 + NO        = NO2 + ACETOL + HOCH2CO           : {%TrG} KRO2NO * (1.-alpha_AN(9,3,1,0,0,temp,cair));
<G45161c> IE3O2 + NO        = IE3ONO2                          : {%TrG} KRO2NO * (alpha_AN(9,3,1,0,0,temp,cair));
<G45161d> IE3O2 + HO2       = IE3OOH {+O2}                     : {%TrG} 0.5*k_RO2_HO2(temp,5);
<G45161e> IE3O2 + HO2       = OH + ACETOL + HOCH2CO {+O2}      : {%TrG} 0.5*k_RO2_HO2(temp,5);
<G45161f> IE3O2 {+RO2}      = ACETOL + HOCH2CO + H2O           : {%TrG} k1_RO2tRO2;
#ENDREPLACE
// DEGREDATION OF IE1O2
#REPLACE <>
<G45162a> IE1O2             = HOCH2CHO + MGLYOX + OH           : {%TrG} 8.05E-2 * (temp)**3.81 * EXP(-6055/temp);
<G45162b> IE1O2             = OH + CO + HO12CO3C4              : {%TrG} 2.54E-30 * 1E-33 * (temp)**24.25 * EXP(-1605/temp);
<G45162c> IE1O2 + NO        = NO2 + HOCH2CHO + MGLYOX + HO2    : {%TrG} KRO2NO * (1.-alpha_AN(9,3,1,0,0,temp,cair));
<G45162d> IE1O2 + NO        = IE1ONO2                          : {%TrG} KRO2NO * (alpha_AN(9,3,1,0,0,temp,cair));
<G45162e> IE1O2 + HO2       = IE1OOH {+O2}                     : {%TrG} 0.5*k_RO2_HO2(temp,5);
<G45162f> IE1O2 + HO2       = OH + HOCH2CHO + MGLYOX + HO2     : {%TrG} 0.5*k_RO2_HO2(temp,5);
<G45162g> IE1O2 {+RO2}      = HOCH2CHO + MGLYOX + H2O          : {%TrG} k1_RO2tRO2;
#ENDREPLACE
```

S2.1.3. IEPOX aqueous-phase

The reactive uptake of IEPOX and subsequent reactions are based on Riedel et al. (2016) and D'Ambro et al. (2017). Riedel et al. investigated the branching ratio between methylbutane-1,2,3,4-tetrol (MT) (see Fig. S4, top) and further products after the acid-catalyzed hydration (ring-opening) of IEPOX. The model considers the formation of triols and oxolane diols. Additionally, the ring-opening by sulfate is implemented, resulting in organosulfate (OS) formation (see Fig. S4, bottom). At high MT or OS mixing ratios, acid-catalyzed oligomerization is further possible. Rate constants are based on the kinetic assessment of D'Ambro et al. (2017) (see supplemental information). MT is expected to be reactive especially against OH. We developed a degradation scheme following estimations and simplifications by (Mouchel-Vallon et al., 2017) and Monod and Doussin (2008). It results in small peroxidic acids and acetol.

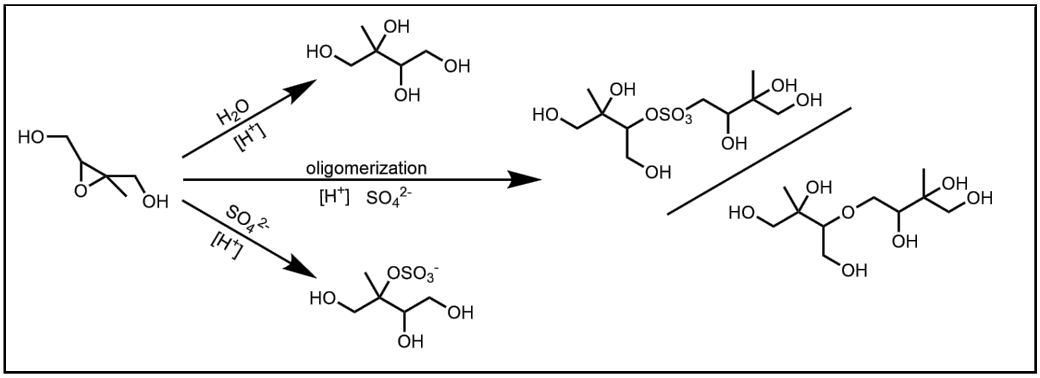

Figure S4. Acid catalyzed ring-opening mechanism of IEPOX in the aqueous phase. Water and sulfate are considered possible nucleophiles, leading to tetrols and organosulfates. Other nucleophiles exhibit slower kinetics. At high IEPOX and tetrol/organosulfate concentration, oligomerization reaction are also accessible. In addition to the products in the scheme, the formation of triols and Tetrahydrofuran (THF) analogs is included in the mechanism.

Fig. S4 mechanism in kpp format:

```
#REPLACE <>
<A45001a_a##> TBIEPOX_a## + H2O_a##          = MEBUTETROL_a##        : {%TrAa##} xaer(##){$} * 0.893 * 5.3E-2 *
c(ind_Hp_a##) *cvfac(##)*cvfac(##);
<A45001b_a##> CBIEPOX_a## + H2O_a##          = MEBUTETROL_a##        : {%TrAa##} xaer(##){$} * 0.893 * 5.3E-2 *
c(ind_Hp_a##) *cvfac(##)*cvfac(##);

<A9901_a##> SO4mm_a## + TBIEPOX_a##          = IDOSm_a## + OHm_a##   : {%TrAa##} xaer(##){$}* 5.2E-1 *
c(ind_Hp_a##) * cvfac(##) * cvfac(##);
<A9902_a##> SO4mm_a## + CBIEPOX_a##          = IDOSm_a## + OHm_a##   : {%TrAa##} xaer(##){$}* 5.2E-1 *
c(ind_Hp_a##) * cvfac(##) * cvfac(##);

<A40004a_a##> TBIEPOX_a## + MEBUTETROL_a##   = DIMEBUTETROL_a##      : {%TrAa##} xaer(##){$}* 1.3E-5 *
c(ind_Hp_a##) * cvfac(##) * cvfac(##);
<A40004b_a##> CBIEPOX_a## + MEBUTETROL_a##   = DIMEBUTETROL_a##      : {%TrAa##} xaer(##){$}* 1.3E-5 *
c(ind_Hp_a##) * cvfac(##) * cvfac(##);
#ENDREPLACE
```

S2.1.4. NO_3-pathway

The update of isoprene towards NO_3 was based on the work by Vereecken et al. (2021). We restricted the NO_3 addition to C1 due to a total share of 87% of this reaction site. High yield isomers are treated explicitly, affecting the rate constants. Reaction rates of peroxides and NO have been adjusted to the general CAABA/MECCA scheme (see Tab. S1). The NO_3 and O_2 addition yields, after the formation of the C2 and C4 nitrate peroxides, mainly epoxides (ring closure). Additionally, a decomposition similar to the previous mechanism is implemented. This is an extension to the previous scheme due to the additional ring closure pathways and more recent rate constants. A decrease of glyoxal, methylglyoxal, and α-nitrooxyacetone, but an increase of different C5 nitrates, and hydroperoxides is expected.

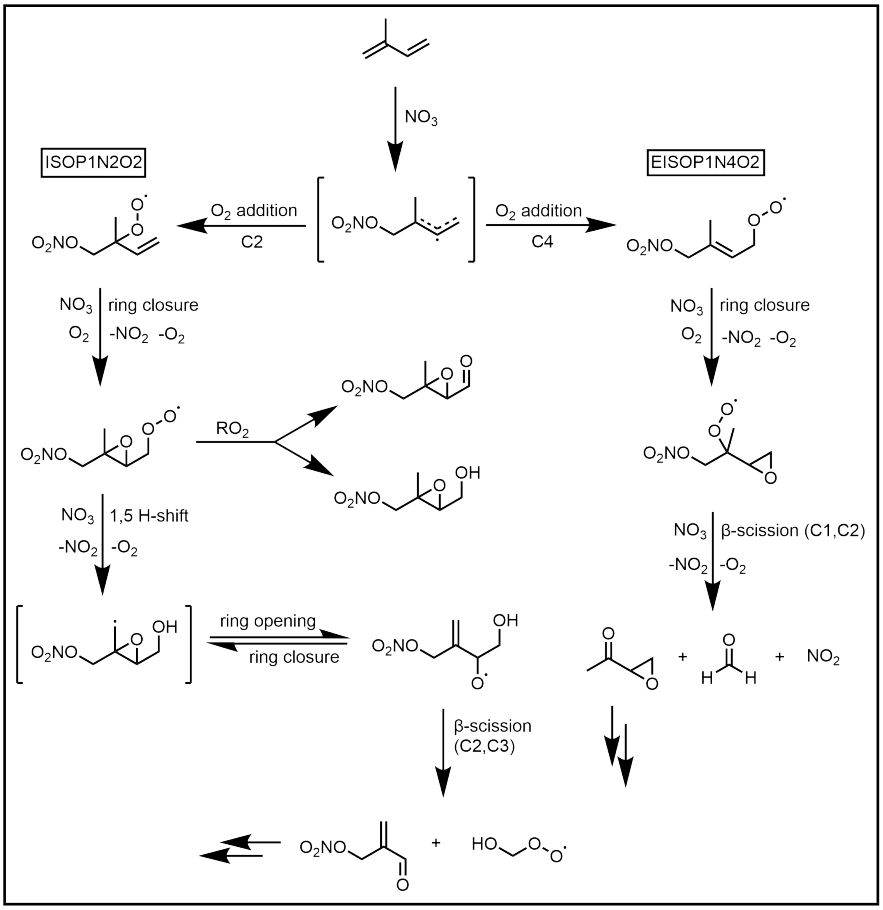

Figure S5. Simplified subset of the updated isoprene + NO_3 mechanism. Only the mechanism for the trans-isomer, formed by the addition of NO_3, is shown. This accounts for 50% of the products (initial trans-isomer). The cis-isomer is implemented as well and yields similar products.

Fig. S5 mechanism in kpp format:

```
#REPLACE <>
<G45564> C5H8 + NO3            = 0.5 CNISOP1N + 0.5 TNISOP1N   : {%TrG} 2.95E-12 * EXP(-450/temp);
#ENDREPLACE

// Nitrate in C1 position

#REPLACE <>
<G45567a> TNISOP1N + O2         = ISOP1N2O2                    : {%TrG} 3.0E-12;
<G45569a> TNISOP1N + O2         = EISOP1N4O2                   : {%TrG} 2.5E-12 * EXP(-450/temp);
<G45566b> ISOP1N2O2             = CNISOP1N {+O2}               : {%TrG} 4.26E20*temp**(-1.80)*exp(-10293/temp);
<G45567b> ISOP1N2O2             = TNISOP1N {+O2}               : {%TrG} 4.68E19*temp**(-1.48)*exp(-9713/temp);
<G45568b> EISOP1N4O2            = TNISOP1N {+O2}               : {%TrG} 2.40E15*temp**(-0.40)*exp(-8707/temp);

// O-abstractions from E/Z-Organic nitrate-peroxy radicals

<G45570> EISOP1N4O2 + NO        = EISOP1N4O + NO2              : {%TrG} KRO2NO * (1.-alpha_AN(9,3,0,0,0,temp,cair));
<G45571> EISOP1N4O2 + NO        = EISOP1N4ONO2                 : {%TrG} KRO2NO * (alpha_AN(9,3,0,0,0,temp,cair));
<G45572> EISOP1N4O2 + NO3       = EISOP1N4O + NO2 {+O2}        : {%TrG} KRO2NO3;
<G45574> EISOP1N4O2 + HO2       = EISOP1N4OOH {+O2}            : {%TrG} k_RO2_HO2(temp, 5) * 1.0;

// E-isomere epoxy-oxy

<G45589> EISOP1N4O {+O2}        = EPXISOPNO2                   : {%TrG} 1.6E12*temp**(-0.01)*exp(-2622/temp);
<G45590> EPXISOPNO2             = EISOP1N4O {+O2}              : {%TrG} 7.5E8*temp**(1.1)*exp(-2556/temp);
<G45583> EPXISOPNO2 + NO        = EPXISOPNO + NO2              : {%TrG} KRO2NO * (1.-alpha_AN(10,3,0,0,0,temp,cair));
<G45584> EPXISOPNO2 + NO        = EPXISOPNONO2                 : {%TrG} KRO2NO * (alpha_AN(10,3,0,0,0,temp,cair));
<G45585> EPXISOPNO2 + NO3       = EPXISOPNO + NO2 {+O2}        : {%TrG} KRO2NO3;
<G45586> EPXISOPNO2 + HO2       = EPXISOPNO + OH {+O2}         : {%TrG} k_RO2_HO2(temp, 5) * 0.5;

// EPXISOPNO chemistry

<G45624> EPXISOPNO              = EPXKET + HCHO + NO2          : {%TrG} 2.38E6 * temp**(2.06) * EXP(-4896/temp);
<G44464> EPXKET + OH            = COHCOCOC                     : {%TrG} k_ads;
<G44465> COHCOCOC               = HOCH2CHO + CH3CO3            : {%TrG} 1.8E13*exp(-20500/(8.314*temp));

// Products from external double bond - O-abstraction

<G45598> ISOP1N2O2 + NO         = ISOP1N2O + NO2               : {%TrG} KRO2NO * (1.-alpha_AN(9,3,0,0,0,temp,cair));
<G45599> ISOP1N2O2 + NO         = ISOP1N2ONO2                  : {%TrG} KRO2NO * (alpha_AN(9,3,0,0,0,temp,cair));
<G45600> ISOP1N2O2 + NO3        = ISOP1N2O + NO2               : {%TrG} KRO2NO3;
<G45601a> ISOP1N2O2 + HO2       = ISOP1N2O + OH                : {%TrG} 0.5*k_RO2_HO2(temp, 5);
<G45601b> ISOP1N2O2 + HO2       = ISOP1N2OOH                   : {%TrG} 0.5*k_RO2_HO2(temp, 5);
<G45601c> ISOP1N2OOH + OH       = ISOP1N2O2                    : {%TrG} 8.38E-12*EXP(390./temp)*0.75;
<G45601d> ISOP1N2O2             = ISOP1N2O                     : {%TrG} k1_RO2tRO2;

// Products from external double bond - beta scission vs ring-closure & O-abstraction

<G45603> ISOP1N2O {+O2}         = LISOP1N23O4R                 : {%TrG} 8.96E9 * temp**0.78 * EXP(-2207/temp) +
4.24E9 * temp**0.92 * EXP(-1996/temp);
<G45604a> LISOP1N23O4R          = ISOP1N2O {+O2}               : {%TrG} 7.42E9 * temp**0.95 * EXP(-2535/temp) +
1.57E10 * temp**0.80 * EXP(-2489/temp);
<G45604b> LISOP1N23O4R + O2     = LISOP1N23O4O2                : {%TrG} 1.5E-11;
<G45605a> LISOP1N23O4O2         = ISOP1CO23O4OOH + NO2         : {%TrG} 3.6E-5;
<G45605b> LISOP1N23O4O2         = LISOP1N23O4O                 : {%TrG} k1_RO2pRO2 * 0.2;
<G45606> LISOP1N23O4O2          = LISOP1N23O4CO                : {%TrG} k1_RO2pRO2 * 0.4;
<G45607> LISOP1N23O4O2          = LISOP1N23O4OH                : {%TrG} k1_RO2pRO2 * 0.4;
<G45608> LISOP1N23O4O2 + NO     = LISOP1N23O4O + NO2           : {%TrG} KRO2NO * (1.-alpha_AN(10,1,0,0,0,temp,cair));
<G45609> LISOP1N23O4O2 + NO     = LISOP1N23O4ONO2              : {%TrG} KRO2NO * (alpha_AN(10,1,0,0,0,temp,cair));
<G45610> LISOP1N23O4O2 + NO3    = LISOP1N23O4O + NO2           : {%TrG} KRO2NO3;
<G45611> LISOP1N23O4O2 + HO2    = LISOP1N23O4O + OH {+O2}      : {%TrG} k_RO2_HO2(temp, 5);
<G45612> LISOP1N23O4O + O2      = LISOP1N23O4CO + HO2          : {%TrG} 2.5E-14 * EXP(-300/temp);

// Products from external double bond - ring-opening

<G45613> LISOP1N23O4O {+O2}     = ISOP1N23O4OH5R               : {%TrG} 3.23E-23 * temp**(10.99) * EXP(400/temp);
<G45615> ISOP1N23O4OH5R         = PMACRO                       : {%TrG} 1.66E8 * temp**(1.33) * EXP(-1652/temp) +
4.04E11 * temp**(0.24) * EXP(-2337/temp);
<G45616> PMACRO                 = ISOP1N23O4OH5R               : {%TrG} 5.74E13 * temp**(-0.49) * EXP(-3440/temp) +
2.09E16 * temp**(-1.40) * EXP(-4227/temp);
<G45617> PMACRO                 = CONO2COCOH + CO + HO2 + HOCH2O2: {%TrG} 1.39E6 * temp**(2.11) * EXP(-1314/temp);
#ENDREPLACE
```

S2.2. Limonene

We implemented limonene and its reaction mechanisms towards the hydroxyl radical, ozone and the nitrate radical. The scheme is based on the MCM (Jenkin et al., 1997). In the OH addition mechanism, the addition to both double bonds is treated and produces lumped peroxides of both isomers at the two addition sites (four possible products). The peroxy radicals reaction with NO, HO_2, NO_3 and by self-reaction. Reaction rates are adjusted to Tab. S1. In the LIMAL reaction mechanism branch (formed from β-scission-induced ring-opening), we added a fast H migration reaction of a resulting C5 product (C517O)(Vereecken and Nozière, 2020). This leads to the production of a methyl hydroxy peroxide rather than a methyl peroxidic acid. Similar adjustments were made in the C923CO3 sub-branch of LIMAL, changing the methacrolein production to hydroxy ethyl peroxidic acid. The LMLKET reaction branch forms C517O, alike the LIMAL mechanism. Thus, this branch is adapted as well. A major change to the mechanism is introduced by the work of Vereecken and Peeters (2012) on β-pinene oxidation. They discovered an intramolecular ring closure reaction for a molecule similar to LIMCO2, formed after the first OH addition (see Fig. S6, left). Prior theoretical investigations by Vereecken and Peeters (2004) have already shown a fast ring closure reaction for unsaturated peroxy radicals. Calculations by Piletic and Kleindienst (2022) revealed that this pathways is not only important for α- and β-pinene, but also for limonene. We implemented the formation and degradation of the ring closure products as presented in the paper with predicted rate constants, but we excluded pathways described as being low yield. Due to the different position of the OH group, the actual rate constant of the reaction step has to be derived and implemented in future updates. The second major difference to the MCM mechanism is the introduction of a second OH addition to the remaining double bond. This addition results in an enhanced nitrate and hydroperoxide formation.

The reactivity of limonene towards ozone is divided into two parts (not shown). The first part covers the creation of the Criegee intermediate at C6 and an aldehyde formation at C1. The following steps are adapted from the MCM with the changes already described for the OH mechanism. The criegee intermediate formation at C7 and the ketone formation at C2 are based on Leungsakul et al. (2005), Carslaw (2013) and Pang et al. (2022). In contrast to the MCM, the adapted mechanism forms NORLIMAL from LIMOOB rather than LIMAL. As a result more ACETOL is formed compared to the MCM. The ozone addition to the non-ring double bond is not considered, which equals a cut-off of 17% (Pang et al., 2022).

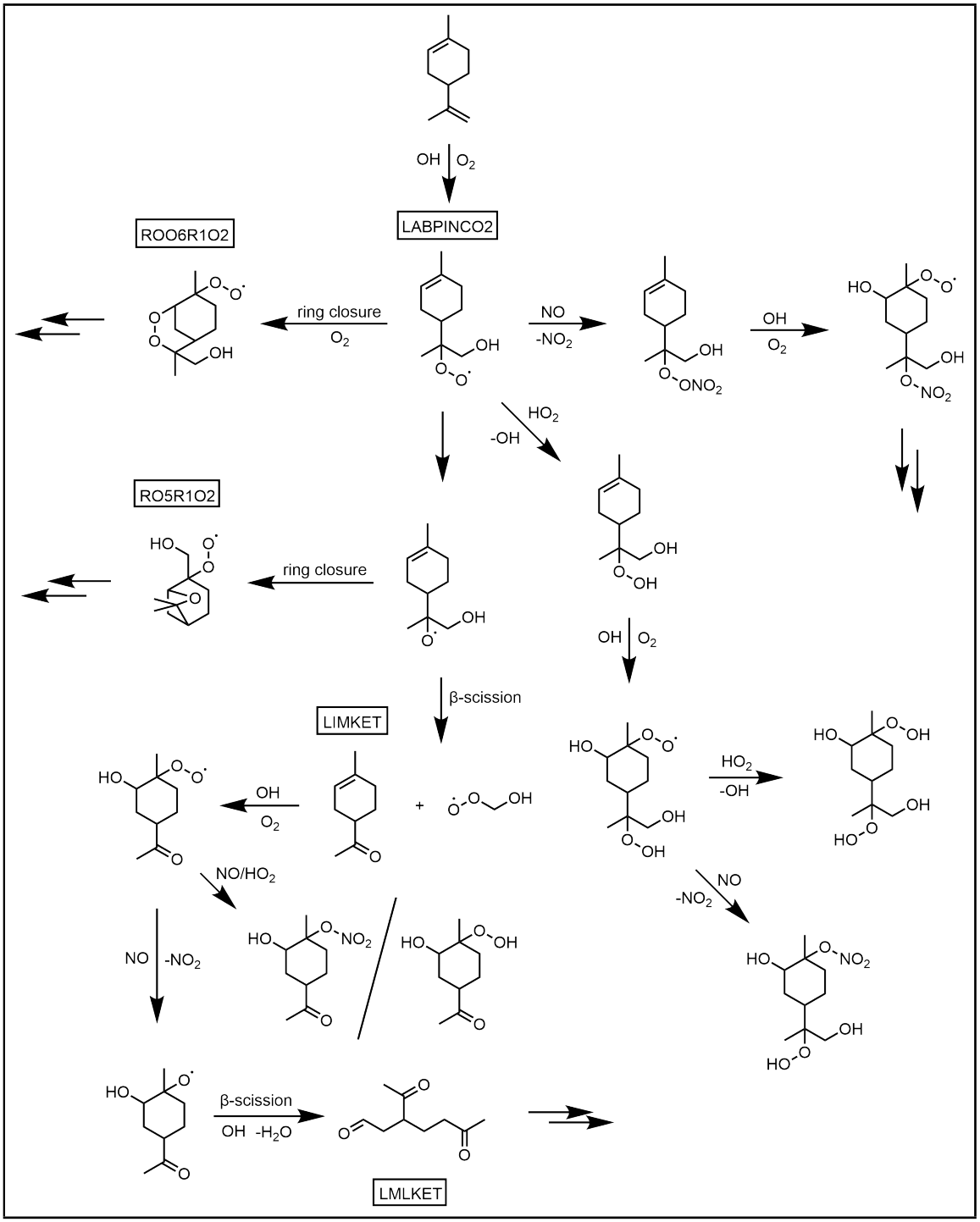

Figure S6. Exemplary cutout of the limonene OH oxidation reaction mechanism. Addition of an hydroxyl radical to the external double bond. The mechanisms also includes further pathways and the addition to the internal double bond.

Fig. S6 mechanism in kpp format:

```
#REPLACE <>
<G40315> LIMONENE + OH {+O2}  = 0.63 LLIMABO2 + 0.37 LABPINCO2 + H2O: {%TrGTer} 3.0E-11 * EXP(515/temp);
#ENDREPLACE

//////////////

#REPLACE <>
<G40336> LABPINCO2 + NO        = LIMCNO3                          : {%TrGTer} KRO2NO*(alpha_AN(11,3,0,0,0,temp,cair));
<G40337> LABPINCO2 + NO        = LABPINCO + NO2                   : {%TrGTer} KRO2NO*(1.-alpha_AN(11,3,0,0,0,temp,cair));
<G40338> LABPINCO2 + HO2       = LIMCOOH {+O2}                    : {%TrGTer} (1-r_CHOHCH2O2_OH)*k_RO2_HO2(temp, 10);
<G40339> LABPINCO2 + HO2       = LABPINCO + OH {+O2}              : {%TrGTer} r_CHOHCH2O2_OH*k_RO2_HO2(temp, 10);
<G40340> LIMCOOH + OH          = LABPINCO2 + H2O                  : {%TrGTer} k_ROOHRO;
<G40341> LABPINCO2 + NO3       = LABPINCO + NO2 {+O2}             : {%TrGTer} KRO2NO3;
<G40342> LABPINCO2             = LABPINCO                         : {%TrGTer} k1_RO2tRO2;
<G40343> LABPINCO2             = ROO6R1O2                         : {%TrGTer} 1.36E9 * EXP(-7097/temp);
<G40344> LABPINCO              = LIMKET + HOCH2O2                 : {%TrGTer} 1.8E13 * EXP(-22380/(8.314*temp));
<G40345> LABPINCO {+O2}        = RO5R1O2                          : {%TrGTer} 1.8E13 * EXP(-15952/(8.314*temp));
#ENDREPLACE

///////////////

#REPLACE <>
<G40346> LIMCNO3 + OH {+O2}    = LABPINCONO2O2                    : {%TrGTer} k_adt;
<G40347> LIMCOOH + OH {+O2}    = LABPINCOOHO2                     : {%TrGTer} k_adt;
<G40348> LABPINCONO2O2 + NO    = LLIMABONO22                      : {%TrGTer} KRO2NO*(alpha_AN(16,3,0,0,0,temp,cair));
<G40349> LABPINCONO2O2 + NO    = LABPINCONO2O + NO2               : {%TrGTer} KRO2NO*(1.-alpha_AN(16,3,0,0,0,temp,cair));
<G40350> LABPINCONO2O2 + NO3   = LABPINCONO2O + NO2               : {%TrGTer} KRO2NO3;
<G40351> LABPINCONO2O2 + HO2   = LLIMABONO2OOH                    : {%TrGTer} k_RO2_HO2(temp, 10);
<G40352> LABPINCONO2O2         = LABPINCONO2O                     : {%TrGTer} k1_RO2tRO2;
<G40353> LABPINCOOHO2 + NO     = LLIMABONO2OOH                    : {%TrGTer} KRO2NO*(alpha_AN(14,3,0,0,0,temp,cair));
<G40354> LABPINCOOHO2 + NO     = LABPINCOOHO + NO2                : {%TrGTer} KRO2NO*(1.-alpha_AN(14,3,0,0,0,temp,cair));
<G40355> LABPINCOOHO2 + NO3    = LABPINCOOHO + NO2                : {%TrGTer} KRO2NO3;
<G40356> LABPINCOOHO2 + HO2    = LLIMABOOH2                       : {%TrGTer} k_RO2_HO2(temp, 10);
<G40357> LABPINCOOHO2          = LABPINCOOHO                      : {%TrGTer} k1_RO2tRO2;
#ENDREPLACE

////////////////////

#REPLACE <>
<G49350> LIMKET + OH {+O2}     = LIMKETO2                         : {%TrGTer} k_adt;
<G49351> LIMKETO2 + NO         = LIMKETONO2                       : {%TrGTer} KRO2NO*(alpha_AN(11,3,0,0,0,temp,cair));
<G49352> LIMKETO2 + NO         = LIMKETO + NO2                    : {%TrGTer} KRO2NO*(1.-alpha_AN(11,3,0,0,0,temp,cair));
<G49353> LIMKETO2 + NO3        = LIMKETO + NO2                    : {%TrGTer} KRO2NO3;
<G49354> LIMKETO2 + HO2        = LIMKETOOH                        : {%TrGTer} k_RO2_HO2(temp, 9);
<G49355> LIMKETO2              = LIMKETO                          : {%TrGTer} k1_RO2tRO2;
<G49356> LIMKETO + OH          = LMLKET + H2O                     : {%TrGTer} 1.8E13 * EXP(-14430/(8.314*temp));
<G40398> LLIMABOOHO            = LIMKETOOH + HOCH2O2              : {%TrGTer} 1.8E13 * EXP(-22380/(8.314*temp));
<G40399> LLIMABONO2O           = LIMKETONO2 + HOCH2O2             : {%TrGTer} 1.8E13 * EXP(-22380/(8.314*temp));
#ENDREPLACE
```

S2.3. Benzene

In a recent investigation, Xu et al. (2020) unraveled new mechanistic information about the benzene OH mechanism. The formation of the first-generation epoxide (BZEPOXMUC), with an 11.8% branching ratio in the MCM and in MECCA, could not be validated. Thus, Xu et al. (2020) proposed the redirection of this reaction channel into the bicyclic hydroxy peroxide formation (BZBIPERO2). With the rising importance of this reaction branch, we additionally performed an update of the following products. Formally, BZBIPERO2 formed glyoxal and 2-furanone. In the new mechanism, the oxygen abstraction at the peroxide opens the peroxide and benzene ring. The resulting functionalized hexene alkoxy radical (Fig. S7, after ring-opening) exhibits two competing intramolecular reactions: β-scission and 1,5 H-shift. The β-scission forms glyoxal and 2-butenedial, while the H-shift yields glyoxal and a ketenol.

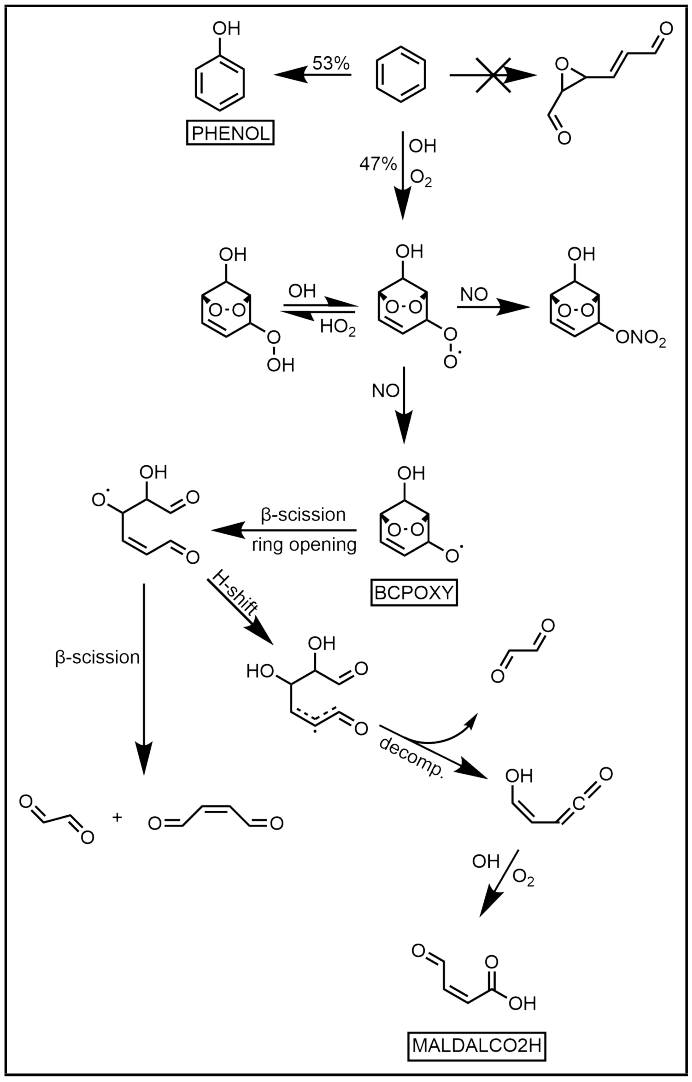

Figure S7. Mechanism of the oxidation of benzene by OH. The initial reaction yielding epoxides is excluded, as it was found to have a very low yield (Xu et al., 2020). The yield was redistributed to the BCP-oxy pathway. Additionally, the BCP-oxy pathway was refined by implementing a new ring-opening reaction and the degradation of the formed product.

Fig. S7 mechanism in kpp format:

```
#REPLACE <G46441>
<G46441> BENZENE + OH         = .53 PHENOL + .47 BZBIPERO2 + .53 HO2  : {%TrGAro} 2.3E-12*EXP(-190./temp);
#ENDREPLACE

#REPLACE <G46522b>
<G46522b> BZBIPERO2  + HO2    = BCPOXY + OH                           : {%TrGAro} k_RO2_HO2(temp,6)*r_BIPERO2_OH;
#ENDREPLACE

#REPLACE <G46523b>
<G46523b> BZBIPERO2  + NO     = BCPOXY + NO2                          : {%TrGAro} KRO2NO*(1.-alpha_AN(9,2,0,0,1,temp,cair));
#ENDREPLACE

#REPLACE <G46524>
<G46524>  BZBIPERO2  + NO3    = BCPOXY + NO2 {+O2}                    : {%TrGAro} KRO2NO3;
#ENDREPLACE

// RING-OPENING

#REPLACE <>
<G46526> BCPOXY               = C6H7O4OXY                             : {%TrGAro} 1.8E13*exp(-21760/(8.314*temp));
<G46527> C6H7O4OXY            = GLYOX + MALDIAL                       : {%TrGAro} 1.8E13*exp(-21760/(8.314*temp));
<G46528> C6H7O4OXY            = KETENOL + GLYOX                       : {%TrGAro} 4E10*exp(-25000/(8.315*temp));
<G44463> KETENOL + OH {+O2}   = MALDALCO2H                            : {%TrGAro} k_ads;
#ENDREPLACE
```

S2.4. Alkanes

MECCA previously included the OH oxidation of methane up to butane. With this update, we extended the scheme up to octane. We used the general alkane mechanism by Atkinson et al. (2008). The mechanism is simplified to prevent the formation of too many compounds and thus save calculational power. But, it can be conveniently extended with more alkanes and detail in future work, if necessary. In the present mechanism, only the H-abstraction at C2 is considered. Applying this simplification, all formed peroxy radicals are converted to alkoxy radicals and perform a 1,5 H-shift as hydrogen in this position is available. This step is ten times slower for pentane than for large alkanes. After dioxygen addition and oxygen abstraction, ether hydroxy nitrates, hydroxy hydroperoxides, or hydroxy ketones (for pentane hydroxy aldehydes) are formed. This scheme is limited to linear alkanes, as branched and cyclic alkanes would exhibit a more complex reaction behavior, thus a unified framework would not be possible.

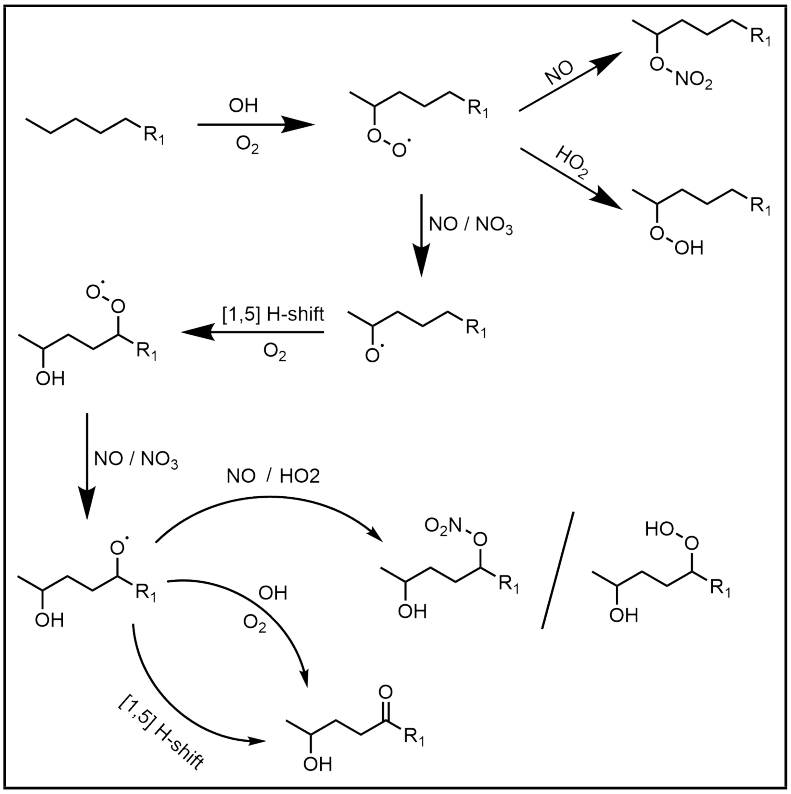

Figure S8. Mechanism of the hexane oxidation yielding hydroperoxides, alkyl nitrates and oxidized hexanes. A similar mechanism is implemented for pentane, heptane and octane.

Fig. S8 mechanism in kpp format:

```
#REPLACE <>
<G46536> C6H14 + OH {+O2}      = C6H13O2 + H2O        : {%TrG} 1.40E-16*temp**1.74*EXP(202./temp); {&3839, 3740} //
<G46537> C6H13O2 + NO          = C6H13O + NO2         : {%TrG} KRO2NO * (1.-alpha_AN(6,2,0,0,0,temp,cair)); {&3840} //
<G46538> C6H13O2 + NO          = HEXBNO3              : {%TrG} KRO2NO * (alpha_AN(6,2,0,0,0,temp,cair)); {&3840} //
<G46539> C6H13O2 + NO3         = C6H13O + NO2 {+O2}   : {%TrG} KRO2NO3; {&3840} // O-abstraction
<G46540> C6H13O2 + HO2         = HEXBOOH {+O2}        : {%TrG} k_RO2_HO2(temp, 6); {&3840} //
<G46541> HEXBOOH + OH          = C6H13O2 + H2O        : {%TrG} k_ROOHRO; {&3840} //
<G46542> C6H13O2               = C6H13O               : {%TrG} k1_RO2sRO2; {&3840} //

////////// H-shift //////////

<G46551> C6H13O {+O2}          = C6OHO2               : {%TrG} 2*4E10*EXP(-3010/temp); {&3840} // [1,5] H-shift, Decomposition is v
<G46552> C6OHO2 + NO           = C6OHO + NO2          : {%TrG} KRO2NO * (1.-alpha_AN(7,2,0,0,0,temp,cair)); {&3840} //
<G46553> C6OHO2 + NO           = HO2C6NO3             : {%TrG} KRO2NO * (alpha_AN(7,2,0,0,0,temp,cair)); {&3840} //
<G46554> C6OHO2 + NO3          = C6OHO + NO2          : {%TrG} KRO2NO3; {&3840} //
<G46555> C6OHO2 + HO2          = HO2C6OOH             : {%TrG} k_RO2_HO2(temp, 6); {&3840} //
<G46556> HO2C6OOH + OH         = HO2C6OOH + H2O       : {%TrG} k_ROOHRO; {&3840} //
<G46557> C6OHO2                = C6OHO                : {%TrG} k1_RO2sRO2; {&3840} //
<G46558> C6OHO + O2            = HO2CO5C6 + HO2       : {%TrG} 2.5E-14*EXP(-300/temp); {&3840, 2419} //
<G46559a> C6OHO {+O2}          = C6ROHOH              : {%TrG} 2*4E10*EXP(-3010/temp); {&3840} //
<G46559b> C6ROHOH + O2         = HO2CO5C6 + HO2       : {%TrG} 2.5E-14*EXP(-300/temp); {&3840, 2419} //
#ENDREPLACE
```

S3. Henry's law solubility constants

Table S2. Newly implemented Henry's law solubility constants H_s estimated by GROMHE, and the temperature-dependence factor $B = \mathrm{d}\ln H_\mathrm{s}/\mathrm{d}(1/T)$ calculated with the method of Kühne et al. (2005). Compounds are characterized by their SMILES string and InChIKey. Only the first block of the InChIKey is shown in the table. As we do not consider stereochemistry here, the last part of the InChIKey is always "-UHFFFAOYSA-N" (excluded for better readability).

compound	**SMILES**	**InChIKey**	H_s **/ M/atm**	$\mathrm{d}\ln H_\mathrm{s}/\mathrm{d}(1/T)$ **/ K**
IEPOX + OH				
IEPOXO4 (LIEPOXO)	CC1(CO)OC1C=O	DNQIATHBSKHPLN	2.1E6	13700
DIEPOXO3 (LDIEPOXO)	CC1(C(=O)CO)CO1	QGQUFAZKBSHWQB	1.3E5	13700
IEPOX1CO3H (LIEPOXCO3H)	CC1(C(=O)OO)OC1O	DJPWYFXNRMHUNU	9.1E4	14400
ME1TRIOL (LTRIOL)	C(O)C(O)C=C(C)(O)	MTMASQITBHTGFW	4.9E9	11100
METHFDIOL	C1C(O)-O-C(O)C1(C)	UNAIOYXCADSMDR	9.1E7	10900
MEBUTETROL	C(O)C(O)C(C)(O)C(O)	HGVJFBSSLICXEM	6.2E12	13600
METRICO	C(O)C(C)(O)C(=O)C(O)	LCGBCDAYKOJPSO	7.4E8	11500
MEDICO4CO	C(=O)C(C)(O)C(=O)C(O)	GXKSWJOBVXKANI	3.1E8	12100
MEDICO1CO	C(=O)C(=O)C(O)(C)C(O)	RRXXDUUNVWXRFN	2.5E9	12100
Isoprene + NO_3				
ISOP1N4OOH (E/Z)	C/C(=C\COO)CON(=O)=O	IRFXVIPRKCCSLU	9.8E4	11400
ISOP1N4ONO2 (E/Z)	C/C(=C\CON(=O)=O)CON(=O)=O	JGJBVRGABXKDRR	2.6E2	9400
HC4CCHO (LHC4ACCHO)	CC(=CCO)C=O	GCHJBJOOADXJFT	1.2E5	10600
EPXISOPNONO2	CC(CON(=O)=O)(ON(=O)=O)C1CO1	UAFKAIYDADHRMX	5.4E3	12500
ISOP1N5ONO2	O=N(=O)OC/C(=C\CO)CON(=O)=O	WRGRJJOKHABEJT	5.9E6	13300
ISOP1N5OOH	O=N(=O)OC/C(=C/CO)COO	LLNBZHMZWYQLAS	2.3E9	14300
ISOP1N6CO	O=C/C(=C\CO)CON(=O)=O	XXORYENTKCFFSM	2.1E7	14000
ISOP1N2ONO2	C=CC(C)(CON(=O)=O)ON(=O)=O	FQSKJUXVWIFNKX	1.6E2	9400
ISOP1N23O4CO (LISOP1N23O4CO)	CC1(CON(=O)=O)OC1C=O	WBVYILWVTRBTDJ	1.5E5	12400
ISOP1N23O4ONO2 (LISOP1N23O4ONO2)	CC1(CON(=O)=O)OC1CON(=O)=O	FSZUIXLMCRZJMS	4.6E3	12500
Large Alkanes + OH				
C5H112ONO2	CC(ON(=O)(=O))CCC	RWRBSYOTDDOXKC	3.4E-1	6000
C5H112O2H	CC(OO)CCCCC(OO)CCC	AXIHYONNAPPFSO	1.4E2	7000
C5OHONO2	C(ON(=O)(=O))CCC(O)C	RIQPKERROQFFJK	2.1E3	9900
C5OHOOH	C(OO)CCC(O)C	GSRFGQMXWRCOMF	7.2E5	10900
C5OHCO	C(O)CCC(=O)C	JSHPTIGHEWEXRW	3.6E5	9800
C6H13ONO2	CC(ON(=O)(=O))CCCC	JLGBOJJVQLNMGV	3.1E-2	6300
C6H13O2H	CC(OO)CCCC	XWXUHAUZCICPHE	1.0E2	7300
C6OHONO2	CC(ON(=O)(=O))CCC(O)C	PAWWQEMXBSLVJC	1.6E3	10200
C6OHOOH	CC(OO)CCC(O)C	BVOYWPYSMMRYPX	5.5E5	11200
C6OHCO	CC(O)CCC(=O)C	ZSDLLTJVENEIDW	2.8E5	10100

Table S2. Newly implemented Henry's law constants estimated by GROMHE, and the temperature-dependence factor $B = \mathrm{d}\ln H_\mathrm{s}/\mathrm{d}(1/T)$ calculated with the method of Kühne et al. (2005). Compounds are characterized by their SMILES string and InChIKey Only the first block of the InChIKey is shown in the table. As we do not consider stereochemistry here, the last part of the InChIKey is always "-UHFFFAOYSA-N" (excluded for better readability). (continued)

compound	SMILES	InChIKey	H_s / M/atm	$\mathrm{d}\ln H_\mathrm{s}/\mathrm{d}(1/T)$ / K
Large Alkanes + OH				
C7H15ONO2	CC(ON(=O)(=O))CCCCC	HHXLSUKHLTZWKR	2.3E-1	6600
C7H15O2H	CC(OO)CCCCC	FWELUXZVATZEMI	7.8E1	7600
C7OHONO2	CCC(ON(=O)(=O))CCC(O)C	MZJHMUSTUUJGSJ	1.2E3	10600
C7OHOOH	CCC(OO)CCC(O)C	KHWIBANUCNWWGW	4.2E5	11600
C72CO5OH (LC7OHCO)	CCC(O)CCC(=O)C	MQRALIJAASQPNT	2.1E5	10500
C8H17ONO2	CC(ON(=O)(=O))CCCCCC	QCOKASLKYUXYJH	6.9E2	7000
C8H17O2H	CC(OO)CCCCCC	NAXZMRYIZGEALQ	5.9E1	8000
C8OHONO2	CCCC(ON(=O)(=O))CCC(O)C	UEQWMROPIQKFIM	9.1E2	10900
C8OHOOH	CCCC(OO)CCC(O)C	QQTSMKQYSKGCOU	3.2E5	11900
C82CO5OH (LC8OHCO)	CCCC(O)CCC(=O)C	KZPPEBIAPHLFQD	1.6E5	10800
Limonene				
HOC2H4CHO	O=CCCO	AKXKFZDCRYJKTF	3.6E3	9900
C517OOH	CC(=O)C(CO)COO	OAFCGFSFCVGKSH	1.1E8	13400
HMVKBCHO	CC(=O)C(C=O)CO	XYGGNMZYIGPNCC	3.6E7	10800
CO2C4CHO	CC(=O)CCC=O	KEHNRUNQZGRQHU	5.6E4	8400
C519OOH	CC(=O)C(CCO)OO	RDSFTYTWLRHJGZ	1.7E7	13400
C517CHO	CC(=O)C(CO)CC=O	JGHPNZFTVGSLKF	9.6E4	12700
C622OOH	C=C(C)C(CO)COO	GWTGWFHICNOSTQ	1.3E6	12000
C519CHO	CC(=O)C(C=O)CCO	PVAHQKAVPKMXGV	2.8E8	11100
C622ONO2	C=C(C)C(CO)CON(=O)=O	UCAFMJJTBHTENA	3.5E3	11000
C622CHO	C=C(C)C(CO)CC=O	JWVBPJJNIHELFZ	5.9E5	11300
C728OOH	CC(CO)(OO)C(CO)CC=O	WJYXJQPIZCIBJO	5.4E12	18100
C727OOH	CC(=O)CCC(OO)C(C)=O	IMCLYNFQESJQRO	2.0E7	12700
C624CHO	C=C(C)C(C=O)CCO	AIMYSSDKEKDSEU	5.9E5	11300
C730OOH	CC(CO)(OO)C(C=O)CCO	YXKHJQXHKYJCPI	6.2E12	18100
C728ONO2	CC(CO)(ON(=O)=O)C(CO)CC=O	CDBHNFBQKSTCON	1.5E10	17100
C622CONO2	C=C(C)C(CO)CC(=O)ON(=O)=O	DJCVHBPUJHAWIU	1.0E5	13900
C730ONO2	CC(CO)(ON(=O)=O)C(C=O)CCO	RVWIAVBELSCRER	3.5E11	17100
C818CO	CC(=O)C(=O)CC(CO)C(C)=O	CRQAGKNTHDNGEW	6.6E8	15900
C816CO	C=C(C)C(=O)CCC(C)=O	FXXXYZSMIIVJDG	3.1E4	10200
C819OOH	CC(=O)CCC(=O)C(C)(CO)OO	JRXMSSDNDAZISI	2.1E9	17000
C817CO	CC(=O)CCC(C=O)C(C)=O	WSCYQCAMZDXSLH	3.1E7	12000
C817OOH	CC(=O)CCC(COO)C(C)=O	WQMXPSRLZZCZTO	1.2E8	13000
C818OOH	CC(=O)C(CO)CC(OO)C(C)=O	DLMBPALZQHFDOH	5.8E10	17000
C729CHO	C=C(C)C(CC=O)CC=O	MEGRLTONSLAOOM	8.1E4	10200
C822OOH	C=C(C)C(CC=O)CCOO	XWYULULFGKWPMD	8.9E5	11300

Table S2. Newly implemented Henry's law constants estimated by GROMHE, and the temperature-dependence factor $B = \mathrm{d}\ln H_\mathrm{s}/\mathrm{d}(1/T)$ calculated with the method of Kühne et al. (2005). Compounds are characterized by their SMILES string and InChIKey Only the first block of the InChIKey is shown in the table. As we do not consider stereochemistry here, the last part of the InChIKey is always "-UHFFFAOYSA-N" (excluded for better readability). (continued)

compound	SMILES	InChIKey	H_s / M/atm	$\mathrm{d}\ln H_\mathrm{s}/\mathrm{d}(1/T)$ / K
Limonene				
C824OOH	C=C(C)C(CCO)C(C=O)OO	FGEKWAMEWUMQIL	8.5E8	15300
RO5R5	CC(C)(OC=O)C(CO)CC=O	MESHXYGXEHAFFE	1.3E7	17300
C819ONO2	CC(=O)CCC(=O)C(C)(CO)ON(=O)=O	XLUWXWLWQTYVOF	4.0E8	16000
C817ONO2	CC(=O)CCC(CON(=O)=O)C(C)=O	ZONZWPKPCIWKRN	4.0E6	12000
C822ONO2	C=C(C)C(CC=O)CCON(=O)=O	JWAJNALJDDSHOA	2.9E3	10300
C824ONO2	C=C(C)C(CCO)C(C=O)ON(=O)=O	YMYILPYDFNRVBZ	9.6E8	14300
C923OOH	C=C(C)C(CCC(C)=O)COO	ZSCOJLRNNZZYOH	1.1E6	11700
C923OH	C=C(C)C(CO)CCC(C)=O	VZYSLJNPEGILSI	5.4E5	12000
NORLIMAL	C=C(C)C(C=O)CCC(C)=O	WPNOYHDEEVPEJH	6.2E4	10600
C924OOH	C=C(C)C(CO)CC(OO)C(C)=O	BVODBOGLMHSHGK	3.0E8	15600
C924OH	C=C(C)C(CO)CC(O)C(C)=O	OXSRPARPRXNCEH	3.8E7	15900
LMLKET	CC(=O)CCC(CC=O)C(C)=O	CWEQHJLFCKMWEE	1.1E8	13000
LIMKET	CC1=CCC(C(C)=O)CC1	HOBBEYSRFFJETF	6.5E1	8000
C817CO3H	CC(=O)CCC(CC(=O)OO)C(C)=O	NVOUBBWYYUIRJW	3.4E9	15900
C822CO3H	C=C(C)C(CC=O)CCC(=O)OO	DRDXOQWGQPPQFG	1.7E6	14200
C822CO2H	C=C(C)C(CC=O)CCC(=O)O	ADULCIYKWVJSFE	4.5E6	14500
C91ONO2	C=C(C)C(CCC(C)=O)CON(=O)=O	JEWJQSHMOKPQHI	3.2E3	10700
NORLIMONO2	CC(=O)CCC(C=O)C(C)(CO)ON(=O)=O	MUTWZANDXPDWFF	3.8E10	16300
C92ONO2	C=C(C)C(CO)CC(ON(=O)=O)C(C)=O	PNFDSIMYWKOAKE	4.8E7	14600
C817CONO2	CC(=O)CCC(CC(=O)ON(=O)=O)C(C)=O	LHFXXFGIVAQFTO	1.2E7	14900
C822CONO2	C=C(C)C(CC=O)CCC(=O)ON(=O)=O	RVFLVBTUEWAABB	6.3E3	13200
BPINCOOH (LABPINCOOH)	CC1=CCC(C(C)(CO)OO)CC1	VVHMRXSQYYKNLC	3.6E6	13400
RO5R1O2H	CC1(C)OC2CC1CCC2(CO)OO	NSOHXIGSWKLSHV	1.0E8	16600
RO5R2O2H	CC1(C)OC(OO)CC1CCC(=O)CO	MFXJOKCSTDMZRM	1.8E9	19100
RO5R3O2H	CC(C)(OC=O)C(CCC(=O)CO)COO	IEPFJXDIWPQIRC	7.8E9	21600
RO5R4O2H	CC(C)(OC=O)C(CO)CC(OO)C(=O)CO	YORZXZYHORHTRW	3.6E12	24000
C923CO3H	C=C(C)C(CCC(C)=O)CC(=O)OO	JSHGCXGTVADTAK	2.2E6	14500
LIMONONIC	C=C(C)C(CCC(C)=O)CC(=O)O	NJOIWWRMLFSDTM	5.8E6	14900
LIMAL	C=C(C)C(CC=O)CCC(C)=O	OGCGCISRMFSLTC	4.1E4	10900
LIMALOOH	CC(=O)CCC(CC=O)C(C)(CO)OO	OQLBLHLZVAPRGN	4.4E12	17700
LIMALOH	CC(=O)CCC(CC=O)C(C)(O)CO	ISUQULRVPDSRIP	2.2E12	18000
LIMALAOOH	C=C(C)C(CC=O)CC(OO)C(C)=O	DVORBFWFCUOYLW	2.5E7	14500
LIMALAOH	C=C(C)C(CC=O)CC(O)C(C)=O	VNYSFQVUCPNMDZ	3.1E6	14900
LIMALACO	C=C(C)C(CC=O)CC(=O)C(C)=O	OXUPJDFJWCMZMO	4.4E6	13400
LIMALBOOH	C=C(C)C(CC=O)CCC(=O)COO	DCWLKDSHBWMMQU	2.4E7	14500
BPINCONO2 (LABPINCONO2)	CC1=CCC(C(C)(CO)(ON(=O)(=O)))CC1	ZELLOEPLERCREX	8.7E3	18800

Table S2. Newly implemented Henry's law constants estimated by GROMHE, and the temperature-dependence factor $B = \mathrm{d}\ln H_\mathrm{s}/\mathrm{d}(1/T)$ calculated with the method of Kühne et al. (2005). Compounds are characterized by their SMILES string and InChIKey Only the first block of the InChIKey is shown in the table. As we do not consider stereochemistry here, the last part of the InChIKey is always "-UHFFFAOYSA-N" (excluded for better readability). (continued)

compound	SMILES	InChIKey	H_s / M/atm	...
Limonene				
C9CONO2	C=C(C)C(CCC(C)=O)CC(=O)(ON(=O)(=O))	FNVMVXZLPDKVAS	8.1E3	19900
LIMALONO2	CC(=O)CCC(CC=O)C(C)(CO)(ON(=O)(=O))	FDBNDHKWTKEDSC	1.3E10	23000
LIMONO2	C=C(C)C(CC=O)CCC(=O)CON(=O)=O	DEKWHDOXDJNWRD	3.9E6	13500
LIMAB15ONO22 (LLIMABONO22)	CC(CO)(ON(=O)=O)C1CCC(C)(ON(=O)=O)C(O)C1	UNHNJOVXNACOSQ	3.1E9	18200
LIMAB15ONO2OOH (LLIMABONO2OOH)	CC(CO)(OO)C1CCC(C)(ON(=O)=O)C(O)C1	JBKULLYZCMWERK	5.1E11	19200
LIMAB15OOH2 (LLIMABOOH2)	CC(CO)(OO)C1CCC(C)(OO)C(O)C1	IRUZCTPAAZATQM	2.3E14	20200
LIMAB1ONO2 (LLIMABONO2)	C=C(C)C1CCC(C)(ON(=O)=O)C(O)C1	LZDKYYHMAURBIK	8.5E3	12400
LIMAB1OOH (LLIMABOOH)	C=C(C)C1CCC(C)(OO)C(O)C1	FPMDSGWWEURSNO	3.6E6	13400
ROO6R1ONO2	CC1(CO)OOC2CC1CCC2(C)ON(=O)=O	JOFCABYMPNXMIS	1.4E4	15200
ROO6R1OOH	CC1(CO)OOC2CC1CCC2(C)OO	GBBPAXKBVMQHIG	6.9E6	16300
ROO6R5ONO2	CC(=O)CCC(CC(=O)ON(=O)=O)OO	LNWOWXJMUJHMJJ	1.7E7	15300
ROO6R5OOH	CC(=O)CCC(CC(=O)OO)OO	RAASFOSVQCCDRJ	4.7E9	16300
ROO6R6ONO2	CC(=O)CCC(CON(=O)=O)OO	CRECMHNOVVIMCR	6.2E7	12400
ROO6R6OOH	CC(=O)CCC(COO)OO	QZPUZDFJKAEVLL	2.6E10	13500
ROO6R7ONO2	CC(=O)CCC(CO)ON(=O)=O	COKJDYWOSQONMU	7.6E6	12800
ROO6R7OOH	CC(=O)CCC(CO)OO	UPAWKBDHGPWUCG	3.3E9	13800
C52COCONO2	CC(=O)CCC(=O)ON(=O)=O	QJXLMYNMVOSKND	6.8E3	11000
C52COCO3H	CC(=O)CCC(=O)OO	COVHHGSUFOHLBW	1.9E6	12000
C624ONO2	C=C(COO)C(CO)(CO)ON(=O)=O	XYBUKFJLXVIRLY	2.0E12	18600
C518OOH	C=C(COO)C(=O)CO	PQEISBQMLHJHJQ	4.2E6	14200
C624OOH	C=C(COO)C(CO)(CO)OO	FUTSLQULSAKEJA	1.2E15	19600
C520ONO2	O=C(CO)C(CO)(COO)ON(=O)=O	ZSADVAXZKGJKSG	2.9E11	20800
BIACETOH2	O=C(CO)C(=O)CO	GJCZUCLKDGABDS	2.1E8	16700
C520OOH	O=C(CO)C(CO)(COO)OO	GRPDYNZWDDUILX	5.4E13	21800
Glyoxal oligomers				
GOLIG1	O=CC(O)-O-C(O)C=O	LEKXYOUPWKVTGM	1.5E14	18700
GOLIG2	O=CC(O)-O-C(O)C(O)O	GWSRJJGBNXJVPO	1.5E17	24000
GOLIG3	OC(O)C(O)-O-C(O)C(O)O	ADECTKUVLJSMDK	3.8E20	28600
Methyl glyoxal oligomers				
MGLYOXDA	CC(=O)C(O)-O-C(O)C(=O)C	QMSLRDMQAWWKIZ	2.0E10	15500
MGLYOXDB	CC(=O)C(O)-O-C(O)(C)C(O)(O)	IUHMFBWAUOLAFM	1.5E15	22400
MGLYFA	CC(=O)C(=O)-O-C(O)C(=O)C	NOUUUBJIFPBZMZ	4.5E6	15600
MGLYFB	CC(=O)C(=O)-O-C(O)(C)C(O)(O)	UCPBJDKPOQEXSQ	7.2E10	22500

S4. Additional model output

S4.1. BASE run with excluded monoterpenes

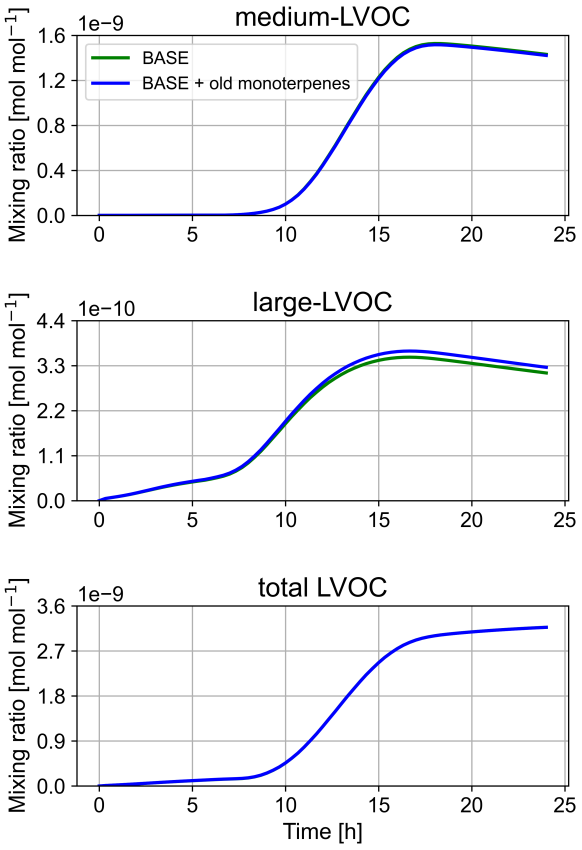

Figure S9. Comparison of the BASE run with a simulation of the BASE run with included carene, camphene and sabinene (old monoterpenes).

S4.2. NO mixing ratios

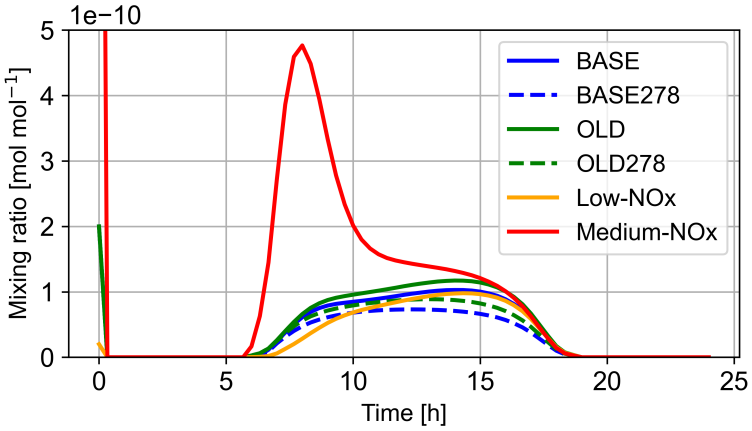

Figure S10. Gas phase mixing ratios of NO during all sensitivity run. High-NO_x was excluded due to especially high mixing ratios (peak value $\sim 1.5 \times 10^{-8}\ mol/mol$).

S4.3. NO2 mixing ratios

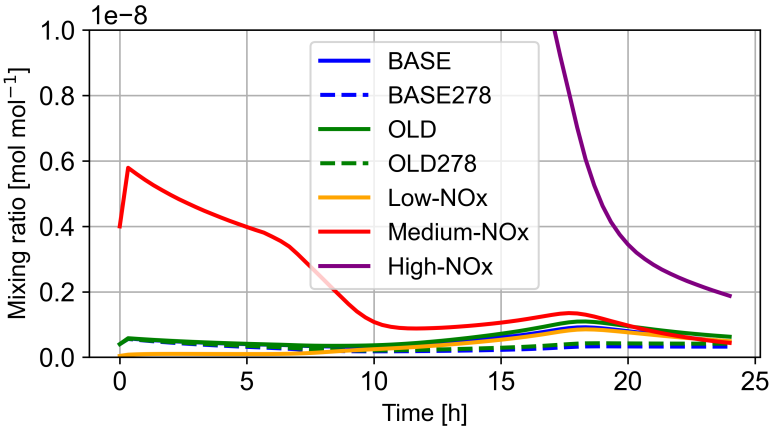

Figure S11. Gas phase mixing ratios of NO_2 during all sensitivity run.

S4.4. NO3 mixing ratios

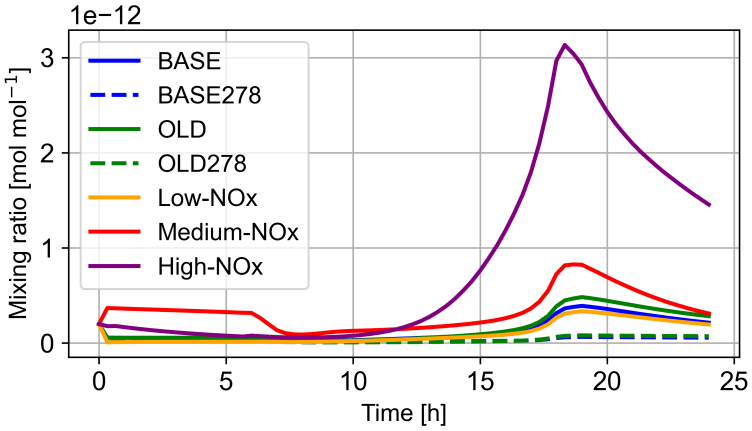

Figure S12. Gas phase mixing ratios of NO_3 during all sensitivity run.

S4.5. OH mixing ratios

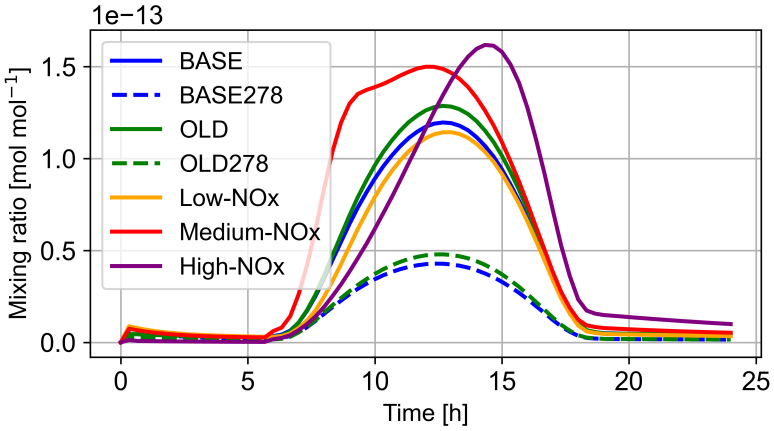

Figure S13. Gas phase mixing ratios of OH during all sensitivity run.

S4.6. O3 mixing ratios

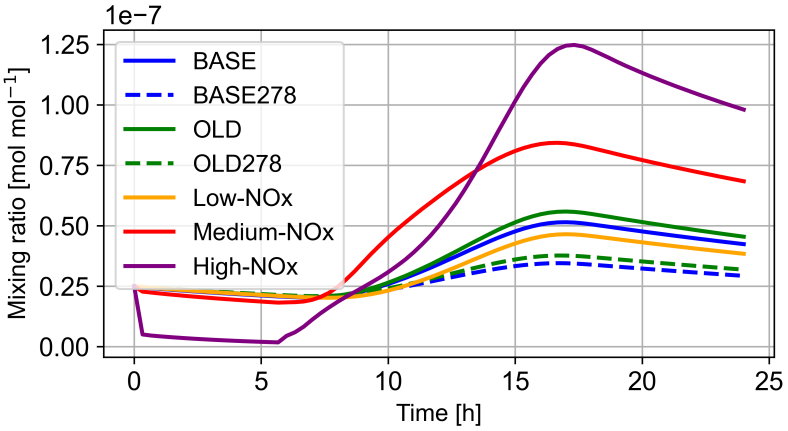

Figure S14. Gas phase mixing ratios of ozone during all sensitivity run.

S4.7. BASE and OLD run pH

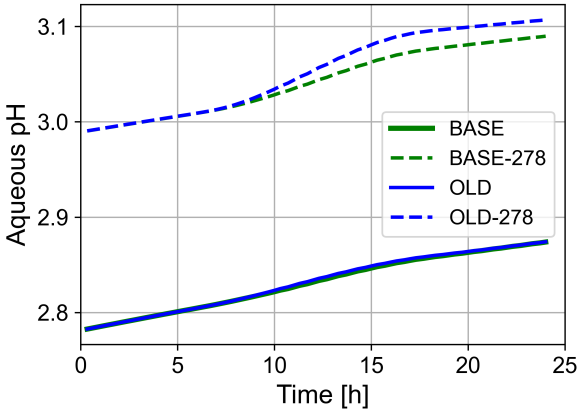

Figure S15. Time dependence of the aqueous pH. The BASE run and the OLD run produce similar acidity's. Thus, their lines overlap. In the SOAS campaign the aerosol pH is approximately 1 (Guo et al., 2015).

S5. Additional data for the comparison to chamber experiments

S5.1. Limonene-ozone

The experiment of limonene-ozone oxidation was part of a measurement campaign to investigate aerosol formation from biogenic VOC (Gkatzelis et al., 2018). In this campaign the oxidation of limonene, β-pinene, their mixture (limonene + β-pinene), and emission from threes and the corresponding formation of aerosols were investigated. In this study, we focused on the limonene oxidation experiment (27.06.2015). The temperature in the chamber during the chosen experiment ranges between 20-26 $^{\circ}\mathrm{C}$. The relative humidity was set to 50 $\%$ at the beginning of the experiment and the roof was closed during the complete experiment. The ALWC was estimated from the high resolution $\mathrm{H_2O}$ signal (v-mode) measured by AMS. This signal can be perturbed by potential interference with the signal of organic compounds. No seeds were injected into the chamber, thus the ALWC is low (≤ 6 µg$/\mathrm{m}^3$) during the full experiments. New particle formation and condensation are likely the dominant SOA formation pathways. Simulations with double/half ALWC do not show an influence on the organic mass. A dilution of 4.8 $\%/\mathrm{h}$ was applied to limonene and ozone mixing ratios. Wall losses of OVOCs and aerosols are a significant processes affecting chamber measurements (Krechmer et al., 2020). Nevertheless, they are uncertain and need to be determined by means of dedicated experiments during each measurement series. Moreover, SAPHIR has a high volume-to-surface ratio that minimizes the losses to the walls. In the main manuscript, we have not considered the wall losses. Figure S18 displays the measured and modeled organic mass with a simplified implementation of aerosol wall loss. The rate constant was estimated based on Schmitt (2018). Figure S17 displays the measured and modeled k(OH). The model depicts a similar trend as the measurements, while the simulation under-predicts the OH reactivity.

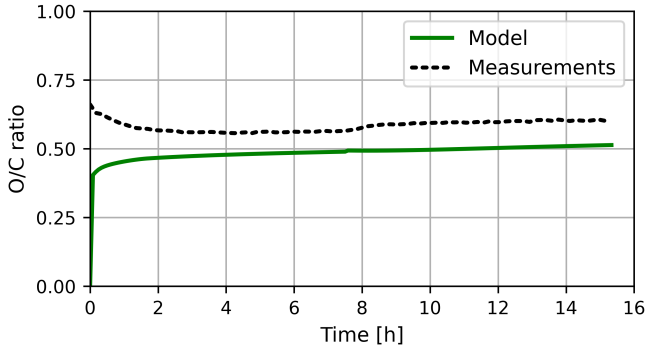

Figure S16. Measured and modeled O/C ratio of the limonene experiment. The measured O/C ratio is corrected by the Canagaratna et al. (2015) approach.

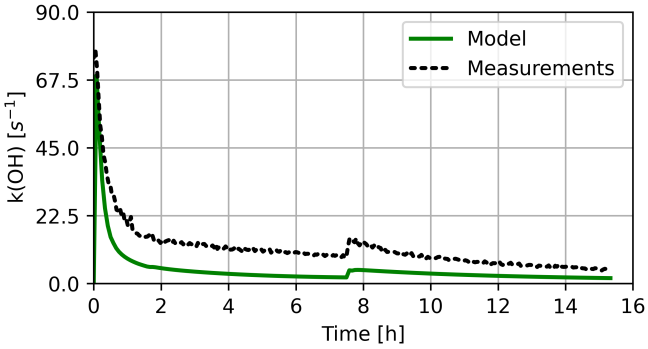

Figure S17. Modeled and measured k(OH) of the limonene experiment.

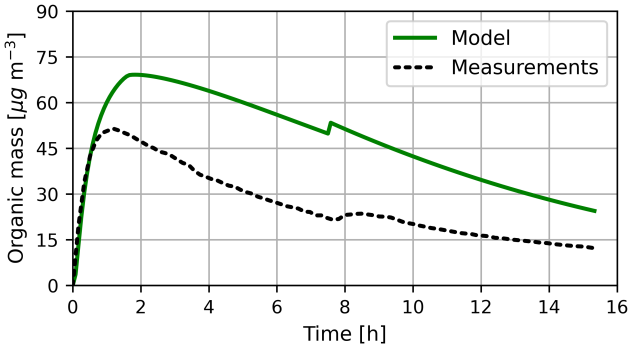

Figure S18. Mass concentration of OM in model and experiment with simplified particle wall loss with a rate of $1.5\times10^{-5}\mathrm{s}^{-1}$. Modeled OM represents all species with an H_s of larger than 4×10^6 M/atm in either gas- or aqueous-phase. This simplification is applied to account for missing processes in the model. After 7.5 h NO is injected into the chamber.

S5.2. Isoprene-NO_3

The isoprene-NO3 campaign in 2018 consists of 15 single experiments, of which eight were carried out in the absence of inorganic seeds and seven with inorganic seeds (Brownwood et al., 2021). We chose the experiment executed on 13^{th} August, as this experiment was also analyzed in Vereecken et al. (2021). The dataset is available in the eurochamp database (Fuchs et al., 2012). In this experiment, no seeds were injected into the chamber and the whole experiment was carried out under dry (RH = 0 %) and dark conditions. The temperature in the chamber during the experiment ranges between 20-27 °C. Further information about the used measurement devices can be found in the SI of Brownwood et al. (2021). The associated model simulation only included gas-phase chemistry, as aerosols can be only formed by new particle formation, which is not included in CAABA/MECCA. NO_3 and HO_2 were constrained to the measurements to ensure the benchmarking of the new mechanism, rather than looking into the model's ability to reflect the chamber radical concentrations. Wall loss of OVOCs is neglected based on the high volume to surface ratio of the SAPHIR chamber. A dilution of 5.6 $\%/\mathrm{h}$ was applied to all species. Isoprene consumed by NO_3 was calculated for the model results as total consumed isoprene, subtracted by the isoprene consumed by OH and ozone.

References

Bates, K. H., Crounse, J. D., St. Clair, J. M., Bennett, N. B., Nguyen, T. B., Seinfeld, J. H., Stoltz, B. M., and Wennberg, P. O.: Gas phase production and loss of isoprene epoxydiols, The Journal of Physical Chemistry A, 118, 1237–1246, https://doi.org/10.1021/jp4107958, 2014.

Brownwood, B., Turdziladze, A., Hohaus, T., Wu, R., Mentel, T. F., Carlsson, P. T., Tsiligiannis, E., Hallquist, M., Andres, S., Hantschke, L., et al.: Gas-particle partitioning and SOA yields of organonitrate products from NO3-initiated oxidation of isoprene under varied chemical regimes, ACS earth and space chemistry, 5, 785–800, 2021.

Canagaratna, M., Jimenez, J., Kroll, J., Chen, Q., Kessler, S., Massoli, P., Hildebrandt Ruiz, L., Fortner, E., Williams, L., Wilson, K., et al.: Elemental ratio measurements of organic compounds using aerosol mass spectrometry: characterization, improved calibration, and implications, Atmospheric Chemistry and Physics, 15, 253–272, 2015.

Carslaw, N.: A mechanistic study of limonene oxidation products and pathways following cleaning activities, Atmospheric Environment, 80, 507–513, https://doi.org/10.1016/j.atmosenv.2013.08.034, 2013.

Cope, J. D., Abellar, K. A., Bates, K. H., Fu, X., and Nguyen, T. B.: Aqueous photochemistry of 2-Methyltetrol and erythritol as sources of formic acid and acetic acid in the atmosphere, ACS Earth and Space Chemistry, 5, 1265–1277, https://doi.org/10.1021/acsearthspacechem.1c00107, 2021.

D'Ambro, E. L., Møller, K. H., Lopez-Hilfiker, F. D., Schobesberger, S., Liu, J., Shilling, J. E., Lee, B. H., Kjaergaard, H. G., and Thornton, J. A.: Isomerization of second-generation isoprene peroxy radicals: Epoxide formation and implications for secondary organic aerosol yields, Environmental science & technology, 51, 4978–4987, https://doi.org/10.1021/acs.est.7b00460, 2017.

Fuchs, H., Novelli, A., Cho, C., Rohrer, F., Tillmann, R., Reimer, D., Hohaus, T., Turdziladze, A., Dewald, P., Liebmann, J. M., Friedrich, N., Shenolikar, J., Schuladen, J., Crowley, J., Brown, S. S., Bernard, F., Zhou, L., Mentel, T., Wu, R., and Hamilton, J. F.: Atmospheric simulation chamber study: isoprene + NO3 - Gas-phase oxidation - product study - 2018-08-13 (Version 1.0) [Data set], https://doi.org/10.25326/BSA7-WX31, 2012.

Gkatzelis, G. I., Tillmann, R., Hohaus, T., Müller, M., Eichler, P., Xu, K.-M., Schlag, P., Schmitt, S. H., Wegener, R., Kaminski, M., et al.: Comparison of three aerosol chemical characterization techniques utilizing PTR-ToF-MS: a study on freshly formed and aged biogenic SOA, Atmospheric Measurement Techniques, 11, 1481–1500, 2018.

Guo, H., Xu, L., Bougiatioti, A., Cerully, K. M., Capps, S. L., Hite Jr, J., Carlton, A., Lee, S.-H., Bergin, M., Ng, N., et al.: Fine-particle water and pH in the southeastern United States, Atmospheric Chemistry and Physics, 15, 5211–5228, 2015.

Jenkin, M., Saunders, S. M., and Pilling, M. J.: The tropospheric degradation of volatile organic compounds: A protocol for mechanism development, Atmos. Environ., 31, 81–104, https://doi.org/10.1016/S1352-2310(96)00105-7, 1997.

Krechmer, J. E., Day, D. A., and Jimenez, J. L.: Always lost but never forgotten: Gas-phase wall losses are important in all teflon environmental chambers, Environmental Science & Technology, 54, 12 890–12 897, 2020.

Kühne, R., Ebert, R.-U., and Schüürmann, G.: Prediction of the temperature dependency of Henry's law constant from chemical structure, Environmental science & technology, 39, 6705–6711, https://doi.org/10.1021/es050527h, 2005.

Leungsakul, S., Jaoui, M., and Kamens, R. M.: Kinetic mechanism for predicting secondary organic aerosol formation from the reaction of d-limonene with ozone, Environmental science & technology, 39, 9583–9594, 2005.

Monod, A. and Doussin, J.: Structure-activity relationship for the estimation of OH-oxidation rate constants of aliphatic organic compounds in the aqueous phase: alkanes, alcohols, organic acids and bases, Atmospheric Environment, 42, 7611–7622, https://doi.org/10.1016/j.atmosenv.2008.06.005, 2008.

Mouchel-Vallon, C., Deguillaume, L., Monod, A., Perroux, H., Rose, C., Ghigo, G., Long, Y., Leriche, M., Aumont, B., Patryl, L., et al.: CLEPS 1.0: A new protocol for cloud aqueous phase oxidation of VOC mechanisms, Geoscientific Model Development, 10, 1339–1362, https://doi.org/10.5194/gmd-10-1339-2017, 2017.

Pang, J. Y. S., Novelli, A., Kaminski, M., Acir, I.-H., Bohn, B., Carlsson, P. T. M., Cho, C., Dorn, H.-P., Hofzumahaus, A., Li, X., Lutz, A., Nehr, S., Reimer, D., Rohrer, F., Tillmann, R., Wegener, R., Kiendler-Scharr, A., Wahner, A., and Fuchs, H.: Investigation of the limonene photooxidation by OH at different NO concentrations in the atmospheric simulation chamber SAPHIR (Simulation of Atmospheric PHotochemistry In a large Reaction Chamber), Atmospheric Chemistry and Physics, 22, 8497–8527, https://doi.org/10.5194/acp-22-8497-2022, 2022.

Paulot, F., Crounse, J. D., Kjaergaard, H. G., Kürten, A., St. Clair, J. M., Seinfeld, J. H., and Wennberg, P. O.: Unexpected epoxide formation in the gas-phase photooxidation of isoprene, science, 325, 730–733, https://doi.org/10.1126/science.1172910, 2009.

Piletic, I. R. and Kleindienst, T. E.: Rates and yields of unimolecular reactions producing highly oxidized peroxy radicals in the OH-induced autoxidation of α-pinene, β-pinene, and limonene, The Journal of Physical Chemistry A, 126, 88–100, 2022.

Riedel, T., Lin, Y.-H., Zhang, Z., Chu, K., Thornton, J., Vizuete, W., Gold, A., and Surratt, J.: Constraining condensed-phase formation kinetics of secondary organic aerosol components from isoprene epoxydiols, Atmospheric Chemistry and Physics, 16, 1245–1254, https://doi.org/10.5194/acp-16-1245-2016, 2016.

Sander, R., Baumgaertner, A., Cabrera-Perez, D., Frank, F., Gromov, S., Grooß, J.-U., Harder, H., Huijnen, V., Jöckel, P., Karydis, V. A., et al.: The community atmospheric chemistry box model CAABA/MECCA-4.0, Geoscientific model development, 12, 1365–1385, https://doi.org/10.5194/gmd-12-1365-2019, 2019.

Schmitt, S.: Formation of Secondary Organic Aerosol from Photo-Oxidation of Benzene: a Chamber Study, vol. 412, 2018.

St. Clair, J. M., Rivera-Rios, J. C., Crounse, J. D., Knap, H. C., Bates, K. H., Teng, A. P., Jørgensen, S., Kjaergaard, H. G., Keutsch, F. N., and Wennberg, P. O.: Kinetics and products of the reaction of the first-generation isoprene hydroxy hydroperoxide (ISOPOOH) with OH, The Journal of Physical Chemistry A, 120, 1441–1451, https://doi.org/10.1021/acs.jpca.5b06532, 2016.

Taraborrelli, D., Lawrence, M. G., Crowley, J. N., Dillon, T. J., Gromov, S., Groß, C. B. M., Vereecken, L., and Lelieveld, J.: Hydroxyl radical buffered by isoprene oxidation over tropical forests, Nature Geoscience, 5, 190–193, https://doi.org/10.1038/ngeo1405, number: 3 Publisher: Nature Publishing Group, 2012.

Vereecken, L. and Nozière, B.: H migration in peroxy radicals under atmospheric conditions, Atmospheric chemistry and physics, 20, 7429–7458, https://doi.org/10.5194/acp-20-7429-2020, 2020.

Vereecken, L. and Peeters, J.: Nontraditional (per) oxy ring-closure paths in the atmospheric oxidation of isoprene and monoterpenes, The Journal of Physical Chemistry A, 108, 5197–5204, 2004.

Vereecken, L. and Peeters, J.: A theoretical study of the OH-initiated gas-phase oxidation mechanism of β-pinene (C 10 H 16): first generation products, Physical Chemistry Chemical Physics, 14, 3802–3815, https://doi.org/10.1039/c2cp23711c, 2012.

Vereecken, L., Carlsson, P., Novelli, A., Bernard, F., Brown, S., Cho, C., Crowley, J., Fuchs, H., Mellouki, W., Reimer, D., et al.: Theoretical and experimental study of peroxy and alkoxy radicals in the NO 3-initiated oxidation of isoprene, Physical Chemistry Chemical Physics, 23, 5496–5515, https://doi.org/10.1039/D0CP06267G, 2021.

Xu, L., Møller, K. H., Crounse, J. D., Kjaergaard, H. G., and Wennberg, P. O.: New insights into the radical chemistry and product distribution in the OH-initiated oxidation of benzene, Environmental Science & Technology, 54, 13 467–13 477, https://doi.org/10.1021/acs.est.0c04780, 2020.